LOCAL DEFORMATION PROPERTIES OF SAND SPECIMENS IN TRIAXIAL LIQUEFACTION TESTS EVALUATED BY DIRECT AND INDIRECT OBSERVATIONS

Ryoichiro HOSHINO[1], Yukika MIYASHITA[2], Takeshi SATO[3]
and Junichi KOSEKI[4]

ABSTRACT: In order to establish a methodology to conduct laboratory soil testing on heterogeneous specimens, a procedure to evaluate directly the local deformation properties of sand specimens was developed by using a transparent membrane and adding colored sand particles to the original ones. By combining it with indirect observation based on the image analysis of the membrane deformation, comparison of the two observations could be made on single specimen. The local deformation properties of a dense Toyoura sand specimen evaluated by indirect observation in triaxial liquefaction test up to a double amplitude axial strain of 5% were consistent with those evaluated by direct observation, except for the regions near the top and bottom ends of the specimen.

Key Words: liquefaction, triaxial test, image analysis, local deformation

INTRODUCTION

The deformation of soil specimens in laboratory tests, such as triaxial tests, torsional shear tests and plane strain compression tests, may not be uniform, in particular with heterogeneous specimens as tested by Fauzi and Koseki (2014) among others. In addition, deformation of homogeneous specimens, such as those of dense sands, may be localized in the post-peak region (Yoshida et al., 1994; Rechenmacher 2003; Wahyudi et al., 2012 among others). Under such circumstances, it is required to establish a proper methodology by evaluating their local deformation properties.

In view of the above, in the current study, it was attempted to develop a procedure to evaluate directly the local deformation properties of sand specimens by using a transparent membrane and adding colored sand particles to the original ones. The local deformation properties of a dense Toyoura sand specimen in triaxial liquefaction test evaluated by this procedure were compared to those evaluated by indirect observation based on the image analysis of the membrane deformation.

TEST APPARATUS, MATERIAL AND PROCEDURES

A triaxial apparatus as described in detail by Kiyota et al. (2007) was employed. The cylindrical specimen was 75 mm in diameter and 150 mm in height. As shown in Fig. 1a, the side view of the specimen was recorded by using a digital camera with a resolution of 4912*7360 pixels.

---

[1] Graduate student, Dept. of Civil Engineering, The University of Tokyo
[2] Technical support specialist, Institute of Industrial Science, The University of Tokyo
[3] Technical director, Integrated Geotechnology Institute Ltd.
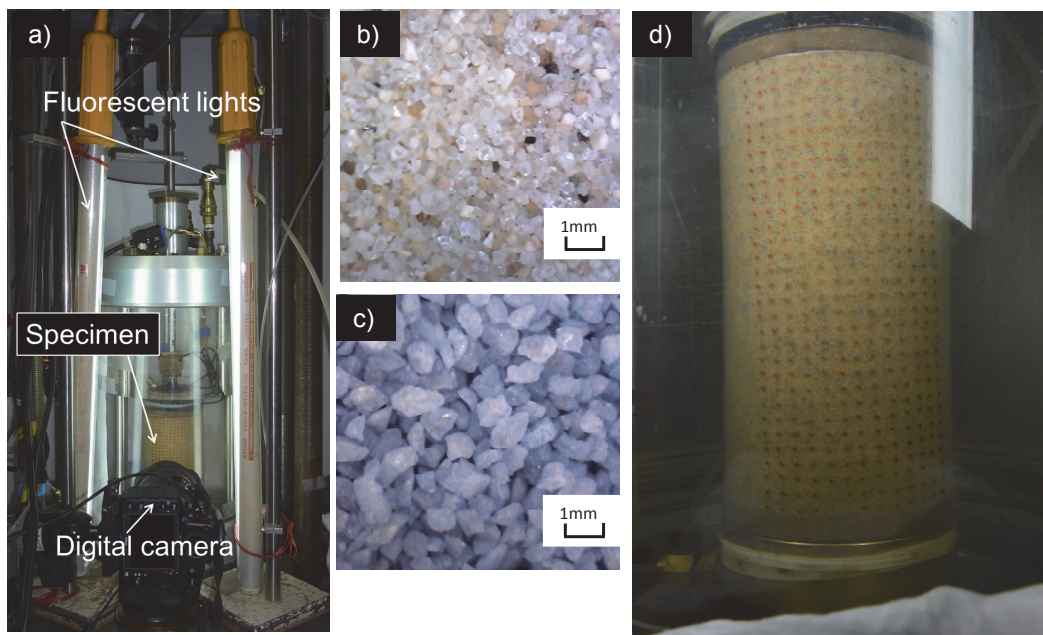[4] Professor, Institute of Industrial Science, The University of Tokyo

Figure 1. a) Setting of digital camera and lights, b) Toyoura sand particles, c) blue-colored sand particles and d) typical side view of specimen using transparent membrane with red dots

Toyoura sand with a mean particle diameter (D_{50}) of about 0.2 mm exhibiting yellowish color as shown in Fig. 1b was used as the test material. In order to make direct observation, blue-colored silica sand particles with D_{50} of about 0.5 mm were mixed with the Toyoura sand particles at a mass ratio of 5%. Figure 1c shows the coarse blue-colored sand particles before mixing. As the transparent membrane, a silicone-rubber sheet having a thickness of 0.5 mm was glued into a cylindrical shape (Ishimaru et al., 2011), on which red dots were painted at a spacing of 5 mm for the purpose of indirect observation, as shown in Fig. 1d.

The specimen consisted of ten compacted layers and was prepared in a mold by the wet-tamping method, where a pre-determined amount of the mixed material at a water content of 15 % was compacted by using a cylindrical tamper with a diameter of about 15 mm into the target thickness to achieve an initial relative density in the range of about 70 to 80%. It was frozen in a freezer and then de-molded. After setting the frozen specimen into the triaxial apparatus and applying a confining stress of 30 kPa by using a partial vacuum as the back pressure, it was thawed and then saturated by using the double vacuuming method (Ampadu and Tatsuoka, 1993). Subsequently, it was consolidated isotropically to a confining stress of 100 kPa and subjected to undrained cyclic axial loading with a single amplitude deviator stress of 80 kPa.

Since the axial loading system was motor-driven, a constant axial strain rate of 0.1 %/min. was employed for the cyclic loading, and digital photos were taken at an interval of 1 min.

As summarized in Fig. 2, the digital photos were recorded in RAW format originally, which were converted into TIFF (Tagged Image File Format) format for processing the data. In order to contrast the red dots on membrane and blue sand particles, respectively, two sets of image data (to be called as "indirect evaluation data" and "direct evaluation data" herein) were prepared by applying the following filtering process:

$(R_{ij}', G_{ij}', B_{ij}')$ = (255, G_{ij}, 255) for indirect evaluation and (R_{ij}, 255, 255) for direct evaluation

where (R_{ij}, G_{ij}, B_{ij}) and $(R_{ij}', G_{ij}', B_{ij}')$ are the intensity scale (from 0 to 255) of the red, green and blue

components before and after the filtering process, respectively. Subsequently, these data sets were converted into gray scale data while enhancing their dynamic range. Typical results from each of these data processing steps are shown in Figs. 3 and 4 for the whole image and a close-up image, respectively.
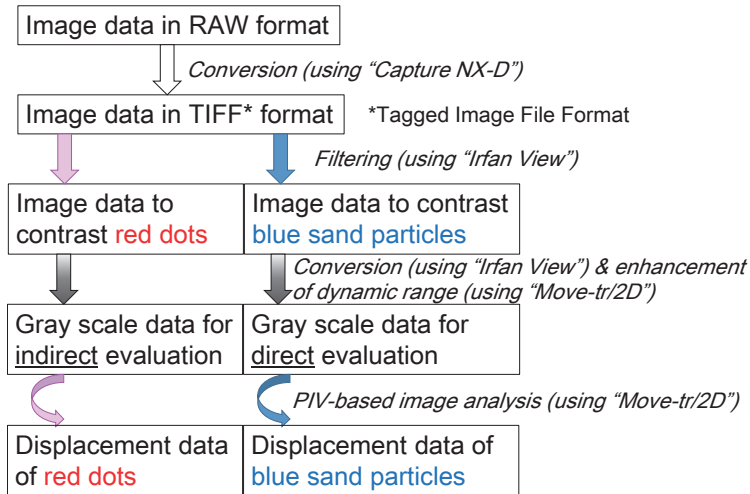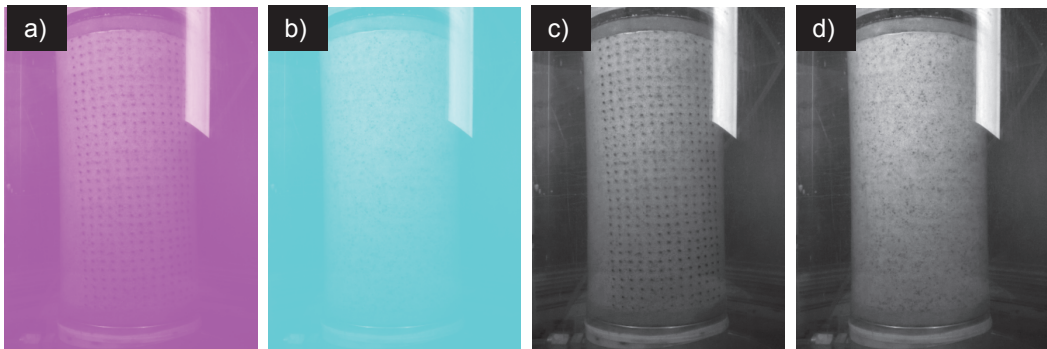

Figure 2. Processing of image data

Figure 3. Typical results from data processing; a) after filtering to contrast the red dots, b) after filtering to contrast the blue sand particles, c) after converting the indirect evaluation data shown in a) into gray scale with enhancement of dynamic range, and d) after converting the direct evaluation data shown in b) into gray scale with enhancement of dynamic range
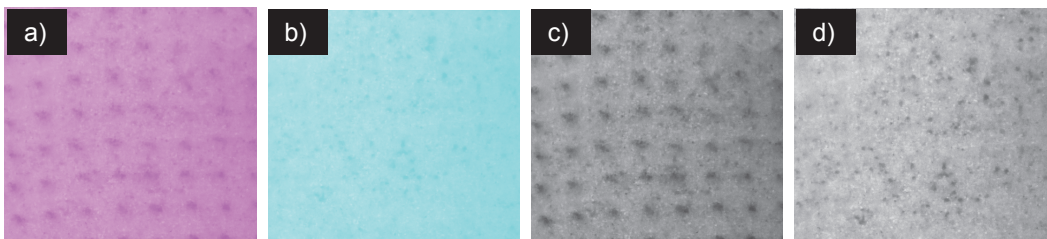

Figure 4. Partial close-up of the results shown in Fig. 2; a) indirect and b) direct evaluation data after filtering, and c) indirect and d) direct evaluation data after converting into enhanced gray scale
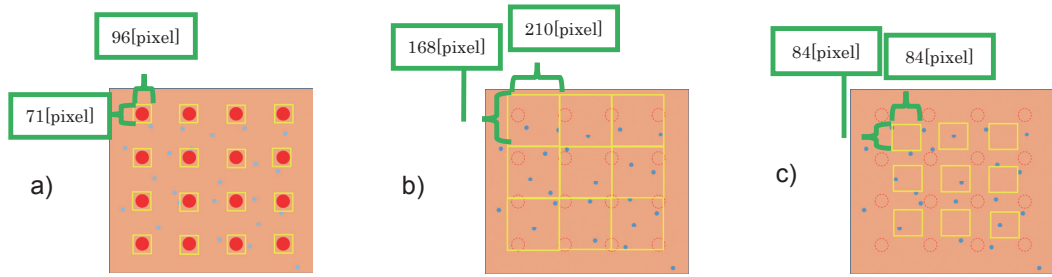
Figure 5. Regions traced in PIV-based analyses; a) indirect evaluation and b) direct evaluation of full grid patterns covering the whole area, and c) direct evaluation of patterns excluding the red dot regions

For the indirect and direct evaluation, PIV (Particle image velocimetry)-based analyses of the two sets of data in enhanced gray scale were conducted to trace the movement of the image patterns made by each of the red dots on the membrane and by the group of the blue sand particles, respectively. As shown in Fig. 5a, a region consisting of 71*96 pixels was used to trace each of the red dot patterns for the indirect evaluation. For the direct evaluation, on the other hand, two different regions were used; one region consisted of 168*210 pixels to trace each of the full grid patterns covering the whole area as shown in Fig. 5b, and the other region consisted of 84*84 pixels that excludes the red dot regions as shown in Fig. 5c. Finally, based on the distribution of local displacements evaluated by these analyses, local strain distribution was computed and compared among the indirect and direct evaluation.

It should be noted that, in order to compare between the indirect and direct evaluation results in a simplified manner, no geometric corrections in terms of the distortion of the image caused by cylindrical shape of the specimen as well as the lens effect (Fauzi and Koseki, 2014) were made in this study. For more quantitative assessment of the local deformation, these corrections would be required.
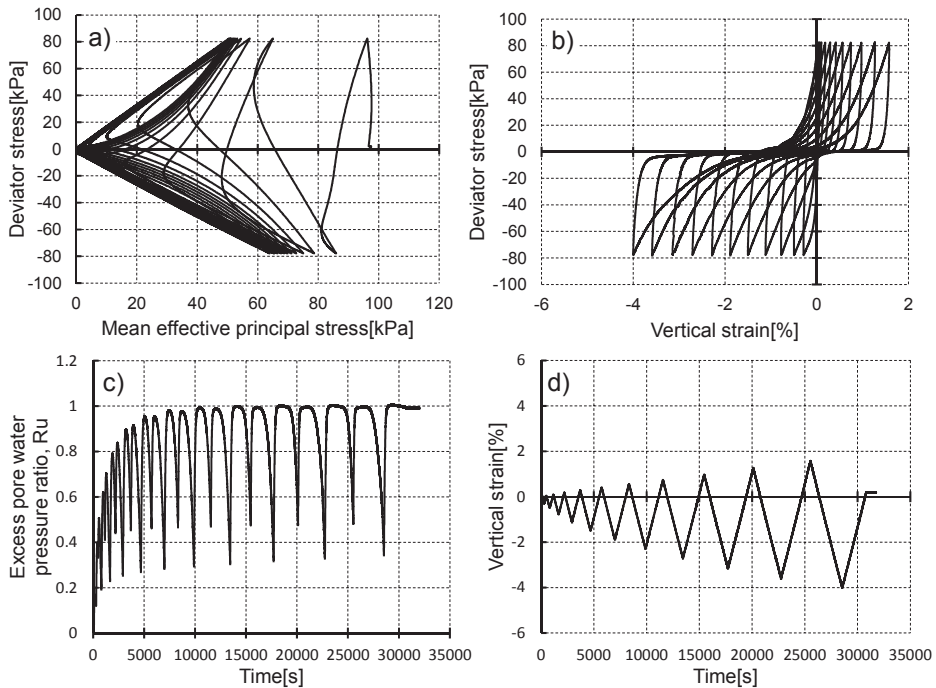

Figure 6. Behavior observed during undrained cyclic loading; a) effective stress path, b) stress-strain relationships and time histories of c) excess pore water pressure ratio and d) global axial strain

TEST RESULTS AND DISCUSSIONS

The behavior observed during the undrained cyclic loading is shown in Fig. 6 in terms of the the effective stress path, stress-strain relationships and the time histories of excess pore water pressure ratio and the global axial strain computed based on the data measured with the external displacement transducer. The excess pore pressure ratio, defined as the ratio of excess pore water pressure to the initial effective stress (=100 kPa), accumulated with the cyclic loading and reached unity, suggesting the occurrence of zero effective stress state or initial liquefaction. It was followed by gradual increase in the axial strain amplitude. After the double amplitude vertical strain exceeded 5% in the 11th cycle, the loading was terminated.

   The results from the image analyses to trace the red dots on the membrane (indirect evaluation) and the blue sand particles (direct evaluation of full grid patterns including the red dots, as shown in Fig. 5b) are compared in Fig. 7 in terms of the vertical displacements at nine regions that were arbitrary selected from the upper, middle, and lower rows and the left, central and right columns. In general, good agreement could be obtained between the indirect and direct evaluation results.

   The ratios of the vertical displacements of the above nine regions based on the direct evaluation to those based on the indirect observation are plotted in Fig. 8 versus the double amplitude, DA, of the global vertical strain during each loading cycle. At the upper rows, the ratios were close to unity irrespective of the DA values. At the middle rows, the ratios were stabilized to unity after the DA values exceeded 1 %. At the lower rows, on the other hand, the ratios deviated from unity to larger extents, since the vertical displacements at these locations were much smaller than those at higher locations.
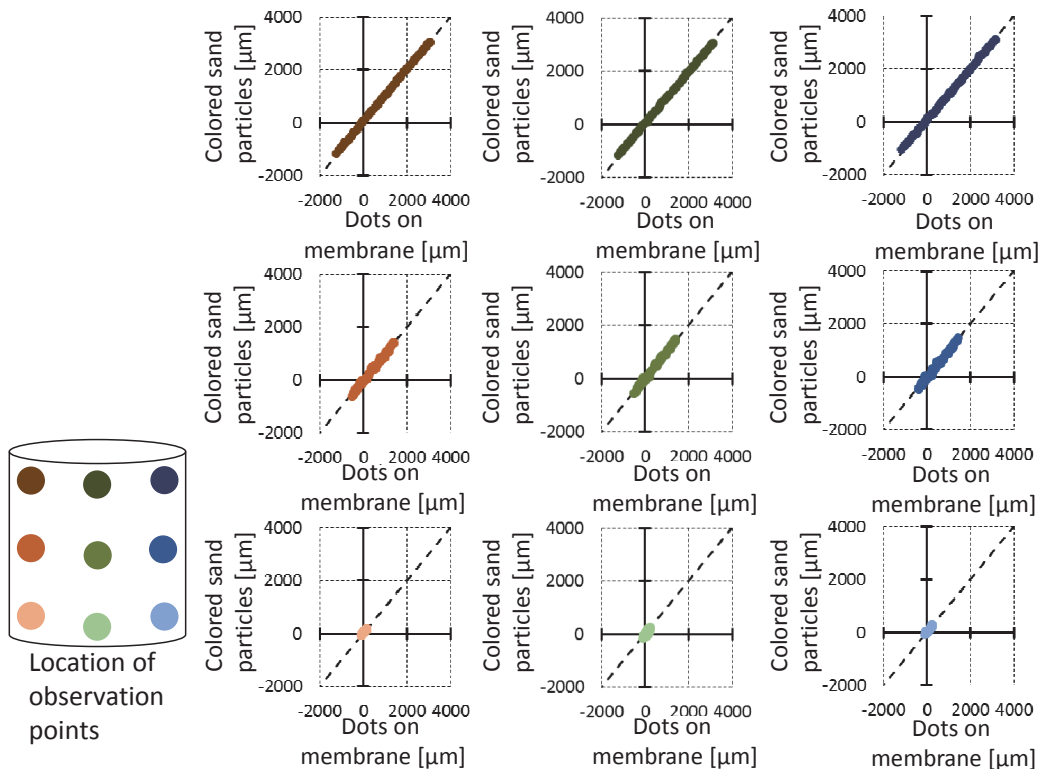

Figure 7. Comparison of vertical displacements at selected points obtained by tracing dots on membrane (indirect evaluation) and sand particles (direct evaluation of full grid patterns, Fig. 6b)
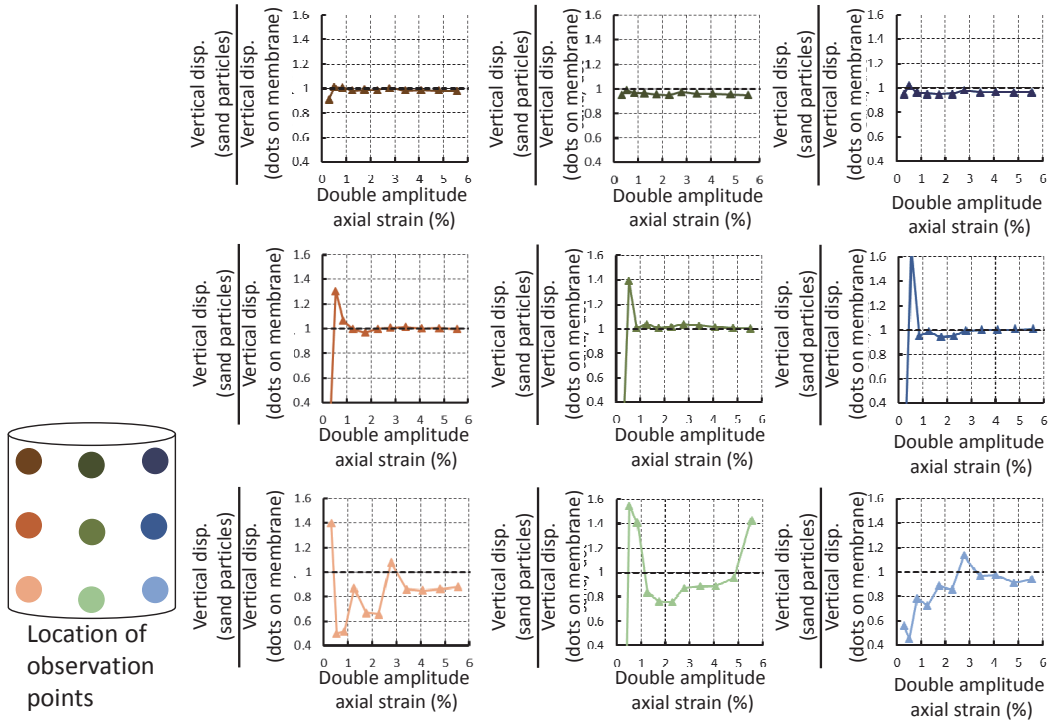
Figure 8. Relationships between ratio of vertical displacements at selected points by indirect and direct evaluation and double amplitude vertical strain in every loading cycle
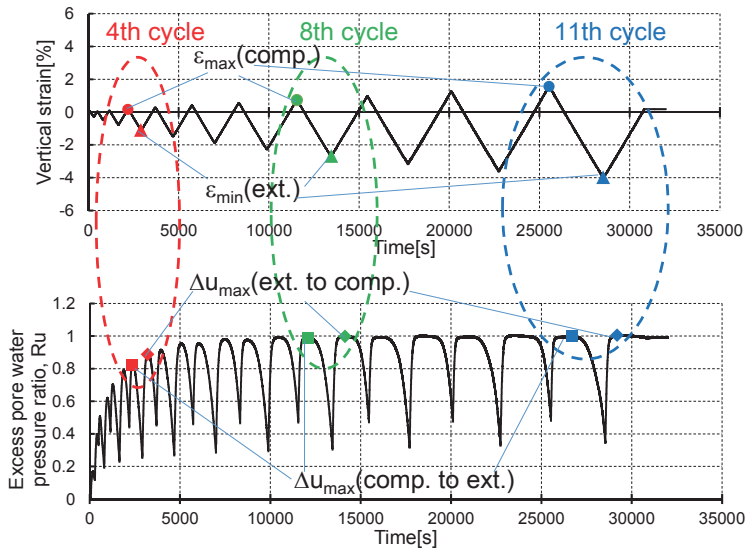

Figure 9. Definition of characteristic states during 4th, 8th and 11th cycles when the distributions of local strain are compared (Figs. 10 through 12 and 14)

Based on the distribution of vertical displacements obtained by the indirect evaluation (Fig. 5a) and two kinds of direct evaluation (Figs. 5b and 5c), three sets of distribution of local vertical strains were computed. By selecting four characteristic states (i.e., the states when the vertical strain became the

maximum and the minimum, and those when the excess pore pressure ratio exhibited the peak values, as defined in Fig. 9), comparisons are made among the three sets of vertical strain distributions in Figs. 10 to 12 during 4th, 8th and 11th loading cycles where the DA value exceeded 1%, 3% and 5%, respectively.
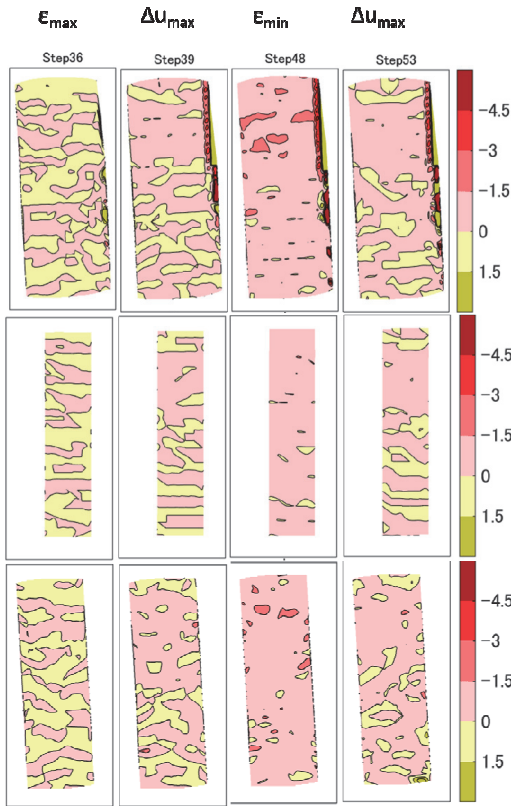

Figure 10. Distributions of local vertical strain during 4th loading cycle; a) indirect evaluation, b) direct evaluation of full grid patterns and c) direct evaluation excluding dot regions

Figure 11. Distributions of local vertical strain during 8th loading cycle; a) indirect evaluation, b) direct evaluation of full grid patterns and c) direct evaluation excluding dot regions
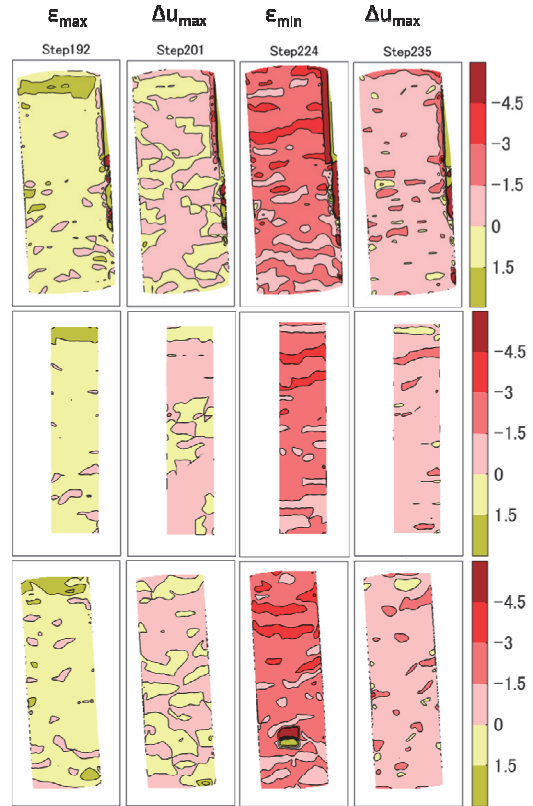
It can be seen from Figs. 10 to 12 that the distributions of the local vertical strain evaluated directly by the two methods as shown in Figs. 5b and 5c were consistent with each other, suggesting that the existence of red dots on the membrane would not affect the direct observation results. In addition, results from indirect observation (Fig. 5a) were also consistent with those from the above direct observations, except for the regions A through C as marked by using colored circles in Fig. 12. The results from the indirect observation by using red dots on the membrane in the regions near the top and bottom ends of the specimen (regions A and C in Fig. 12) may not be reliable, due to excessive deformation of the membrane near the bottom end that was filled by sand particles as shown in Fig. 13a, and possibly to formation of water film near the top end as can be inferred from the photo shown in Fig. 13b. The authors could not identify the reason for the exceptionally large local strain values observed in region B based on the direct observation excluding the red dots.

In Fig. 14, another comparison is made in terms of the distribution of the local horizontal strain during the 11th loading cycle. The effects of the excessive deformation of the membrane near the bottom end (region C, Fig. 13a) could be also observed, while the results from the indirect observation were in general consistent with those from the direct observations.
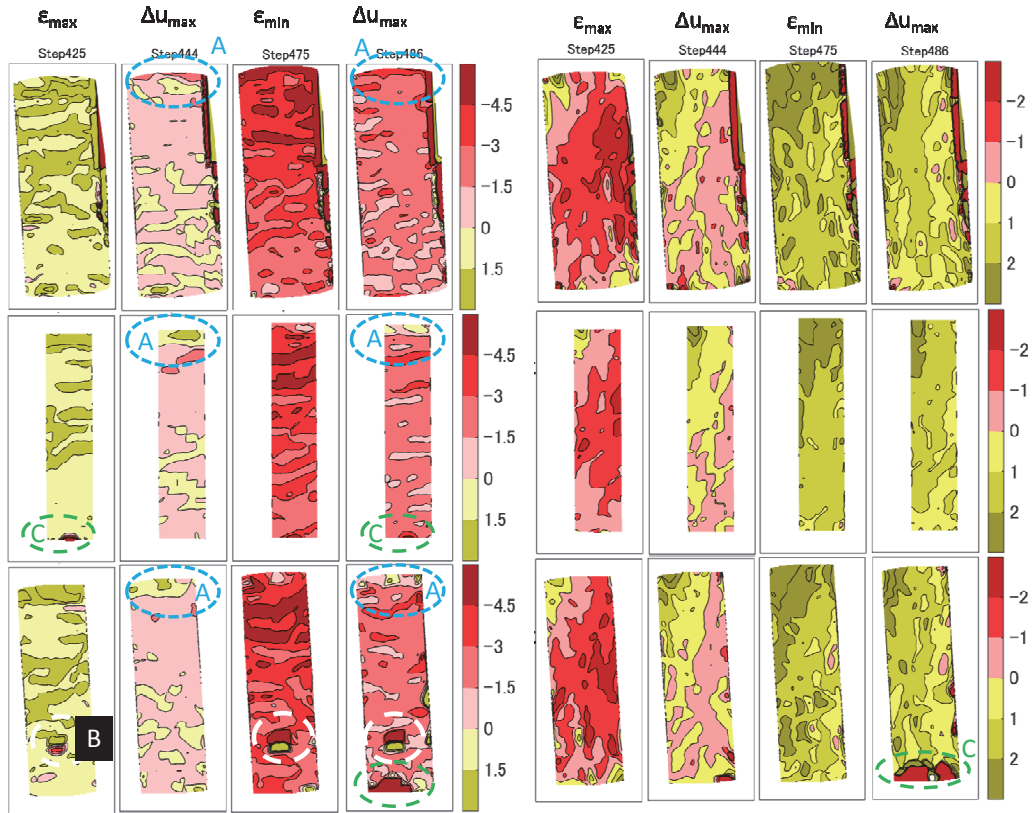
Figure 12. Distributions of local vertical strain during 11th loading cycle; a) indirect evaluation, b) direct evaluation of full grid patterns and c) direct evaluation excluding dot regions

Figure 14. Distributions of local horizontal strain during 11th loading cycle; a) indirect evaluation, b) direct evaluation of full grid patterns and c) direct evaluation excluding dot regions
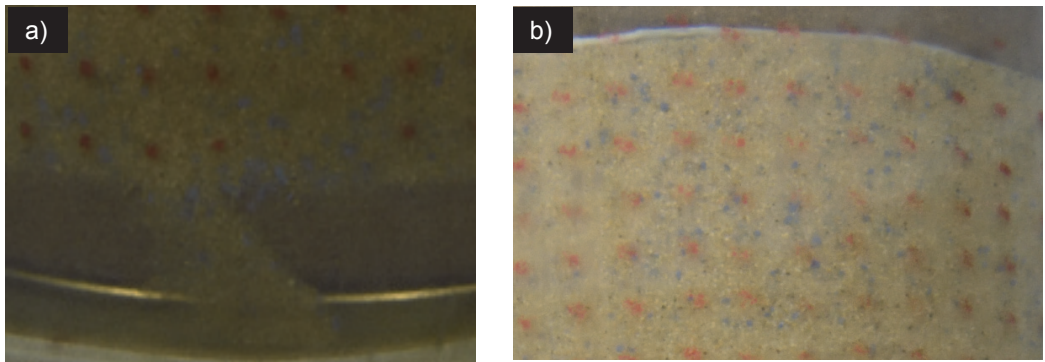

Figure 13. a) Excessive deformation of the membrane near the bottom end that was filled by sand particles, and b) possible formation of water film near the top end (the white-colored sheet located on the upper part of this photo is a filter paper, below which a thin cavity layer could be observed under the states when the excess pore water pressure ratio became unity.)

It should be noted that possible effect of the stratification that was created during the specimen preparation by compaction in ten layers using the wet-tamping method could be seen in Figs. 10 to 12, in which alternative formation of horizontal stripes appeared in the distributions of local vertical strain. In the distribution of local horizontal strain, on the other hand, such effect was not observed, as typically seen in Fig. 14.

CONCLUSIONS

The results from the current study can be summarized as follows:

1) A procedure to evaluate directly the local deformation properties of sand specimens was developed by using a transparent membrane and adding colored sand particles to the original ones. By combining it with indirect observation based on the image analysis of the membrane deformation, comparison of the two observations could be made on single specimen.

2) The local deformation properties of a dense Toyoura sand specimen evaluated by indirect observation in triaxial liquefaction test up to a double amplitude axial strain of 5% were consistent with those evaluated by direct observation, except for the regions near the top and bottom ends of the specimen.

3) The results from indirect observation of the regions near the top and bottom ends of the specimen may not be reliable, due possibly to formation of water film near the top end and excessive deformation of membrane near the bottom end.

REFERENCES

Ampadu, S.K. and Tatsuoka, F. (1993): "Effect of setting method on the behaviour of clays in triaxial compression from saturation to undrained shear", *Soils and Foundations*, 33(2), 14-34.

Fauzi, U.J. and Koseki, J. (2014): "Local deformation properties of segregated sand specimen in hollow cylindrical torsional shear tests", *Bulletin of ERS*, 47, 27-36.

Ishimaru, M., Sawada, M., Koseki, J. and Miyashita, Y. (2011): "Failure behavior of artificial rock masses with discontinuities in plane strain compression tests", *Journal of Japan Society of Civil Engineers*, A2, 67(2), I_293-I_393 (in Japanese).

Kiyota, T. and Koseki, J. (2007): "Effects of sample disturbance on liquefaction resistance and small strain characteristics of sandy soils", *Bulletin of ERS*, 40, 85-97.

Rechenmacher, A. L. (2003): "Imaging-based experimental soil mechanics," *Proceedings of the 1st Japan-US Workshop on Testing, Modelling and Simulation*, ASCE, Geotechnical Special Publication, 143, 653-663.

Wahyudi, S., Miyashita, Y. and Koseki, J. (2012): "Shear banding characteristics of sand in torsional shear test evaluated by means of image analysis technique", *Bulletin of ERS*, 45, 123-130.

Yoshida, T., Tatsuoka, F., Siddiquee, M. S. A., Kamegai, Y. and Park, C.S. (1994): "Shear banding in sands observed in plane strain compression", *Localization and Bifurcation Theory for Soils and Rocks*, Chambon, J Desrues, I. Vardoulakis (eds), Balkema, 165-179.